

## NEAR-ARCSECOND RESOLUTION OBSERVATIONS OF THE HOT CORINO OF THE SOLAR TYPE PROTOSTAR IRAS 16293–2422<sup>0</sup>

S. BOTTINELLI<sup>1,2</sup>, C. CECCARELLI<sup>1</sup>, R. NERI<sup>3</sup>, J. P. WILLIAMS<sup>2</sup>, E. CAUX<sup>4</sup>, S. CAZAUX<sup>5</sup>, B. LEFLOCH<sup>1</sup>, S. MARET<sup>1</sup>, A. G. G. M. TIELENS<sup>6</sup>

*Draft version October 25, 2004*

### ABSTRACT

Complex organic molecules have previously been discovered in solar type protostars, raising the questions of where and how they form in the envelope. Possible formation mechanisms include grain mantle evaporation, interaction of the outflow with its surroundings or the impact of UV/X-rays inside the cavities. In this Letter we present the first interferometric observations of two complex molecules, CH<sub>3</sub>CN and HCOOCH<sub>3</sub>, towards the solar type protostar IRAS16293–2422. The images show that the emission originates from two compact regions centered on the two components of the binary system. We discuss how these results favor the grain mantle evaporation scenario and we investigate the implications of these observations for the chemical composition and physical and dynamical state of the two components.

*Subject headings:* ISM: abundances — ISM: individual (IRAS16293) — ISM: molecules — stars: formation

### 1. INTRODUCTION

Solar type Class 0 protostars are characterized by being observable only at millimeter to far infrared wavelengths. This is because the central forming stars are surrounded and obscured by massive envelopes, making them the coldest known protostars. Yet, the cold envelopes hide inner warm regions where the grain mantles, built during the pre-collapse phase, evaporate. Following gas phase reactions between the evaporated mantle molecules (also called first generation molecules), organic complex molecules (second generation molecules) form in these regions. While this picture has now been widely accepted for massive protostars (see e.g. Kurtz et al. 2000; van Dishoeck & Blake 1998), it is only recently that evidences in support of parts of this scenario have been accumulated for low mass protostars. Actually, so far the existence of inner warm regions with evaporated mantles in solar type protostars has been argued indirectly from the sophisticated analysis of molecular multi-frequency single dish observations (Ceccarelli et al. 2000a,b; Schöier et al. 2002; Maret et al. 2002, 2004; Doty et al. 2004). A survey on almost a dozen of Class 0 sources has shown that, typically, the inner warm regions have sizes of a few tens of AUs (Maret et al. 2004), i.e the size of the Solar

Nebula. Now that the existence of these regions has been demonstrated, the questions of their nature and chemical composition have become relevant because of the link with the formation of our own Solar System. What is the inventory of organic molecules of such regions? What are their origin and evolution? In particular, could these molecules be incorporated into the planet-forming disks surrounding the protostars?

Based on theoretical arguments, no complex, second generation molecules should have the time to form in solar type protostars. The reason is that the gas crossing time of the warm regions is estimated to be much shorter ( $\lesssim 10^3$  yr), than the predicted chemical formation time ( $\gtrsim 10^4$  yr; Schöier et al. 2002). But our theories have somewhere flaws, since complex organic molecules have been detected in the two (out of two) sources where they have been searched for: IRAS16293–2422 (Cazaux et al. 2003) and NGC1333-IRAS4A (Bottinelli et al. 2004). We therefore may even doubt the basic prediction that those molecules originate in the warm inner regions of the envelopes! It is, for example, possible that the process which is responsible for the release in the gas phase of the mantle constituents, is not the thermal evaporation, but the interaction of the outflow with the surroundings, or even of UV/X-rays with the cavities excavated by the outflow (Schöier et al. 2002, 2004). Alternatively, the emission could come from disk surfaces which would have been heated by accretion shocks (Schöier et al. 2004). The proof that the complex organic molecules detected by Cazaux et al. (2003) and Bottinelli et al. (2004) originate from the inner warm regions (envelope or disk), called hot corinos (Ceccarelli 2004; Bottinelli et al. 2004), was still missing until today.

In this Letter we bring the missing proof and report interferometric observations of two complex, second generation molecules, methyl cyanide and methyl formate, towards the prototype of the hot corinos, IRAS16293–2422 (hereafter IRAS16293).

### 2. OBSERVATIONS AND RESULTS

arXiv:astro-ph/0410601 v1 25 Oct 2004

<sup>0</sup> Based on observations carried out with the IRAM Plateau de Bure Interferometer. IRAM is supported by INSU/CNRS (France), MPG (Germany) and IGN (Spain).

<sup>1</sup> Laboratoire d’Astrophysique de l’Observatoire de Grenoble, BP 53, 38041 Grenoble, Cedex 9, France.

sbottine@obs.ujf-grenoble.fr; ceccarel@obs.ujf-grenoble.fr; lefloch@obs.ujf-grenoble.fr; maret@obs.ujf-grenoble.fr

<sup>2</sup> Institute for Astronomy, University of Hawai’i, 2680 Woodlawn Drive, Honolulu HI 96822, USA. jpw@ifa.hawaii.edu

<sup>3</sup> Institut de Radio Astronomie Millimétrique, 300 rue de la Piscine, 38406 Saint Martin d’Hères, France. neri@iram.fr

<sup>4</sup> Centre d’Etude Spatiale des Rayonnements, CNRS-UPS, 9 Avenue du Colonel Roche, BP 4346, 31028 Toulouse, Cedex 4, France. caux@cesr.fr

<sup>5</sup> INAF, Osservatorio Astrofisico di Arcetri, Largo Enrico Fermi, 5 I-50125 Firenze, Italy. cazaux@arcetri.astro.it

<sup>6</sup> Kapteyn Astronomical Institute, P.O. Box 800, 9700 AV Groningen, The Netherlands. tielens@astro.rug.nl

Observations of IRAS16293 ( $\alpha(2000) = 16^{\text{h}}32^{\text{m}}22^{\text{s}}.6$ ,  $\delta(2000) = -24^{\circ}28'33''$ ) were carried out at the IRAM Plateau de Bure Interferometer on February 1<sup>st</sup> and March 25<sup>th</sup> 2004 in the B and C configurations of the array. Five CH<sub>3</sub>CN transitions at 110.4 GHz and 4 HCOOCH<sub>3</sub> transitions at 226.4 GHz were obtained simultaneously, along with the continuum emission at 3 mm and 1.3 mm. The receivers were tuned single side band at 3 mm and double side band at 1.3 mm. CH<sub>3</sub>CN and HCOOCH<sub>3</sub> transitions were covered with two correlator units, each of 40 and 80 MHz bandwidth respectively. Typical system temperature were 250 K (USB) at 3 mm and 500 K (DSB) at 1.3 mm. Phase and amplitude calibrations were obtained by observing the nearby point sources 1514-241 and NRAO 530 every 20 minutes. Bandpass calibration was carried out on 3C273 and 0851+202 and the absolute flux density scale was derived from MWC349, 3C345 and 0923+392. Data calibration was performed in the antenna based manner and uncertainties are less than 10% at 3 mm and less than 20% at 1.3 mm. Flux densities were obtained from visibilities using standard IRAM procedures. Continuum images were produced by averaging line-free channels. Line maps were obtained by cleaning line images after subtraction of the continuum directly from the visibilities.

Figures 1-a and 1-c show the integrated line emission of CH<sub>3</sub>CN and HCOOCH<sub>3</sub>, averaged over all the transitions listed in Table 1 for each molecule. Note that the energy of the upper level of the CH<sub>3</sub>CN transitions decreases with frequency, but that maps averaged over each individual transition do not show any significant difference. This means that the emitting region does not depend on the energy of the transition, i.e. on the excitation conditions (but rather on a jump of the molecular abundances). Continuum emission at 3 and 1.3 mm is displayed in Figures 1-b and 1-d respectively. These maps show two components which are spatially coincident with the centimeter wavelength emission regions A and B mapped by Wooten (1989) and with the millimeter wavelength emission regions MM1 and MM2 mapped by Mundy et al. (1990, 1992). As already noted in the previously mentioned works (see also Looney, Mundy & Welch 2000; Schöier et al. 2004), the south-east region (“source A” or “MM1”) is the weakest in the continuum but brightest in line emission. On the contrary, the north-west region (“source B” or “MM2”) is the brightest in the continuum and weakest in line emission.

Table 1 gives the intensities and sizes of the line and continuum emissions. Within the errors, we recover all the line emission measured by the IRAM 30m (Cazaux et al. 2003).

Finally, the spectra at 1.3 mm of emission regions A and B are shown in Figure 2, assuming a  $V_{\text{LSR}}=3.9$  (Figure 2-a) and  $2.7 \text{ km s}^{-1}$  (2-b) respectively (see discussion in the next section). Again, note that the sum of A and B (Figure 2-c) reproduces very well the features in the spectrum obtained at the IRAM 30m (Cazaux et al. 2003).

### 3. DISCUSSION AND CONCLUSIONS

The most important result of the presented observations is that the complex molecules observed by Cazaux et al. (2003) originate in two compact regions, whose di-

ameters are about  $1.5''$  (A) or less (B), as shown in Figure 1 (and Table 1). This goes along with the fact that the images do not show any evidence of emission associated with the molecular outflows seen at larger scales (see below for the discussion on the line profiles). Also, following the remark in the Introduction, the Plateau de Bure images do not reveal any evidence of emission from cavities excavated from the outflows either. Indeed, the cavities are typically  $\sim 20''$  in size, located  $\sim 30''$  away from the source along the <sup>12</sup>CO outflow (see e.g. Arce & Sargent 2004), which would have been easily detected by the Plateau de Bure. The two regions where the molecular emission comes from, are compact, and while source A is barely resolved in the 1mm images<sup>8</sup>, source B is unresolved. The measured sizes ( $1.5''$  at 160 pc correspond to a radius of about 120 AU) are remarkably consistent with the emission coming from a region where the dust temperature exceeds 100 K in source A (150-200 AU: based on multi-frequency single dish observations: Ceccarelli et al. 2000a,b; Shöier et al. 2002), and therefore, where the grain mantles evaporate. Thus, these observations support the basic prediction (from the modeling of the single dish observations; Ceccarelli et al. 2000a,b; Cazaux et al. 2003) that a hot corino with a radius of about 150 AU exists inside the cold envelope of IRAS16293, and that in that region, complex molecules are formed because of grain mantle evaporation.

In addition to that, the Plateau de Bure observations confirm that the two sources A and B are different, as noted by previous authors (Wooten 1989; Mundy et al. 1990, 1992). They differ in line intensities and extent (Fig. 1), and this corresponds to a difference in their chemical composition. But, before discussing this point, it is necessary to address the second most striking difference in the two sources: their line profiles (Fig. 2). Source A has clearly broadened spectra (FWHM  $\sim 8 \text{ km s}^{-1}$ ), while source B shows apparently much narrower profiles (FWHM  $\sim 2 \text{ km s}^{-1}$ ). Furthermore, the lines of source B seem to peak at  $V_{\text{LSR}}=2.7 \text{ km s}^{-1}$ , whereas the parent cloud velocity is at  $V_{\text{LSR}}=3.9 \text{ km s}^{-1}$  (compatible with the spectra of source A, although given the broad profiles it is difficult to precisely determine the  $V_{\text{LSR}}$  of source A). Note that the cloud’s  $V_{\text{LSR}}$  ( $3.9 \text{ km s}^{-1}$ ) is very nicely measured by the two CN absorption lines in the observed band<sup>9</sup> (Figure 2). As said, no evidence of outflowing gas is seen in the images, and also the broad line profiles of source A are consistent with gas *in-falling* towards a  $\sim 1 M_{\odot}$  object (Ceccarelli et al. 2000a,b; Schöier et al. 2002). Therefore, both the images and line profiles of source A are fully consistent with the hot corino hypothesis.

The case of source B is less obvious: why does this source have narrower lines and why do they peak at  $2.7 \text{ km s}^{-1}$ ? But is this true? A very careful look at the B spectra rises doubts. Indeed, all the B lines have a second small peak —sometimes at the limit of the noise— on the red-shifted side of the spectrum. This second

<sup>8</sup> It is likely that the emission from source A originates in the disk around this source. A detailed study of this aspect is postponed to a forthcoming paper.

<sup>9</sup> The absorption originates in the foreground (envelope + cloud) cold gas, which absorbs the photons emitted in the hot corino regions (the CN emission component, being extended, is filtered out by the interferometric observations).

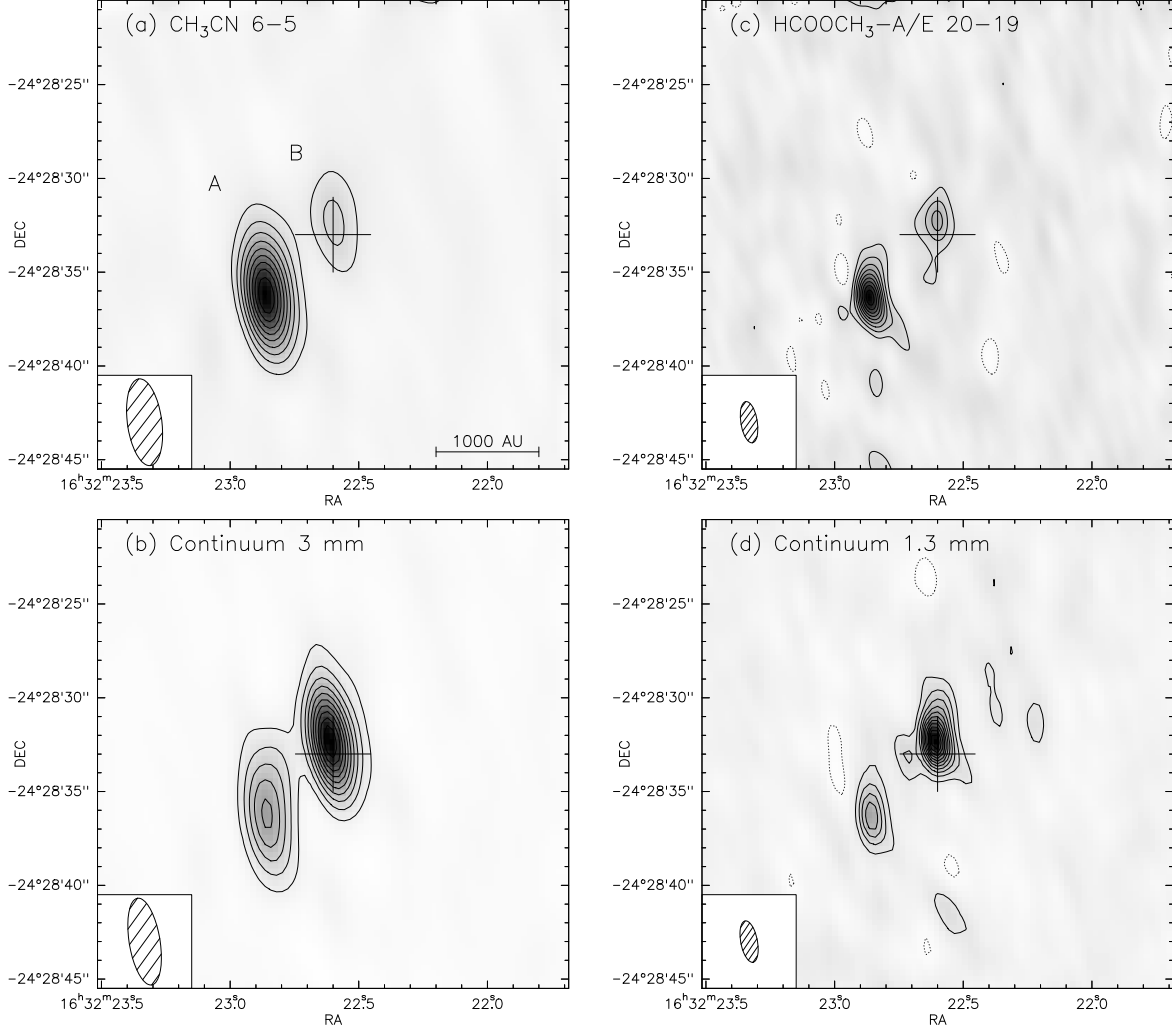


FIG. 1.— (a) Line map of  $\text{CH}_3\text{CN}$ , averaged over the five transitions listed in Table 1; the rms is  $3 \text{ mJy beam}^{-1}$  and contours range from 15 to  $150 \text{ mJy beam}^{-1}$  in steps of  $15 \text{ mJy beam}^{-1}$ . (b) Continuum emission at 3 mm, with an rms of  $3 \text{ mJy beam}^{-1}$ ; contour levels range from 20 to  $220 \text{ mJy beam}^{-1}$  in steps of  $20 \text{ mJy beam}^{-1}$ . (c) Line map of  $\text{HCOOCH}_3\text{-A and -E}$ , averaged over the four transitions listed in Table 1; the rms is  $8 \text{ mJy beam}^{-1}$  and contour levels range from 20 to  $200 \text{ mJy beam}^{-1}$  in steps of  $20 \text{ mJy beam}^{-1}$ . (d) Continuum emission at 1.3 mm, with an rms of  $15 \text{ mJy beam}^{-1}$ ; contour levels range from 50 to  $600 \text{ mJy beam}^{-1}$  in steps of  $50 \text{ mJy beam}^{-1}$ . Beam sizes are  $4''.7 \times 1''.6$  and  $2''.2 \times 0''.9$  at 3 and 1.3 mm respectively.

TABLE 1  
LINE AND CONTINUUM EMISSION

Molecule	Transition	$E_{\text{up}}^{\text{a}}$ ( $\text{cm}^{-1}$ )	Frequency (GHz) or Wavelength	(Integrated) intensity		Size ( $''$ ) <sup>b</sup>		$\Delta\text{RA}, \Delta\text{Dec}$ ( $''$ ) <sup>c</sup>	
				A	B	A	B	A	B
$\text{CH}_3\text{CN}$	$6_{5,0} - 5_{5,0}$	137.1	110.330	1.39(0.09)	0.51(0.06)	0.8(0.2)	< 0.8	3.6, -3.3	-0.0, 1.1
	$6_{4,0} - 5_{4,0}$	92.4	110.350	1.70(0.08)	0.38(0.06)	0.8(0.2)	< 0.8	3.7, -3.2	-0.1, 0.7
	$6_{3,0} - 5_{3,0}$	57.6	110.364	2.75(0.08)	0.67(0.05)	0.9(0.1)	< 0.8	3.7, -3.2	+0.1, 0.6
	$6_{2,0} - 5_{2,0}$	32.8	110.375	2.56(0.08)	0.51(0.05)	1.2(0.1)	< 0.8	3.6, -3.3	+0.1, 0.9
	$6_{1,0,0} - 5_{1,0,0}$	17.9/12.9	110.381/110.383	5.26(0.10)	1.05(0.07)	0.9(0.1)	< 0.8	3.6, -3.3	-0.0, 0.6
$\text{HCOOCH}_3\text{-E/A}$	$20_{2,19} - 19_{2,18}$	83.5	226.713/226.718	6.44(0.41)	3.36(0.36)	$1.4(0.2) \times 0.7(0.1)$	0.8(0.2)	3.6, -3.5	-0.1, 0.7
	$20_{1,19} - 19_{1,18}$	83.5	226.773/226.778	11.13(0.49)	4.05(0.39)	$1.6(0.1) \times 0.8(0.1)$	0.8(0.1)	3.7, -3.3	-0.0, 0.7
continuum			3 mm	0.17	0.26	$3.4 \times 1.4$	$1.5 \times 0.8$	3.5, -2.9	+0.2, 0.7
continuum			1.3 mm	0.77	1.02	$3.7 \times 1.2$	$1.5 \times 0.8$	3.5, -3.3	+0.2, 0.6

NOTE. — The line intensity is in units of  $\text{Jy km s}^{-1}$ , while the continuum is in Jy. Errors are given in parentheses.

<sup>a</sup>Energy of the upper level of the transition.

<sup>b</sup>FWHM of gaussian fit.

<sup>c</sup>Relative peak position from the fit.

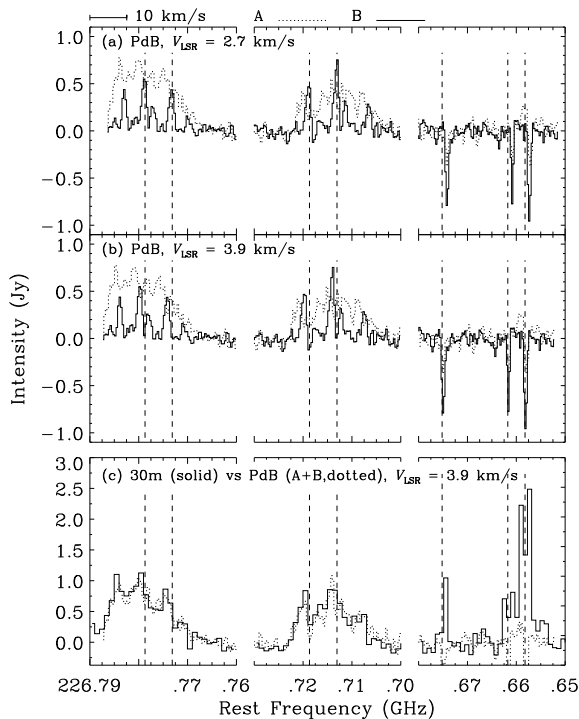


FIG. 2.— (a) Spectra at 1 mm averaged over the emission regions of sources A (dotted line) and B (solid line), and displayed for  $V_{\text{LSR}}=2.7 \text{ km s}^{-1}$ . The velocity resolution is  $0.4 \text{ km s}^{-1}$  and rms are 0.08 and 0.06 Jy for A and B respectively. (b) Same as (a) but with  $V_{\text{LSR}}=3.9 \text{ km s}^{-1}$ . (c) The solid line represents the spectrum obtained at the IRAM 30m (Cazaux et al. 2003) with a velocity resolution of  $1.3 \text{ km s}^{-1}$  and rms of 0.11 Jy. Overlaid in dotted line is the sum of the Plateau de Bure spectra of sources A and B (rms=0.10 Jy). Vertical lines indicate the frequencies of  $\text{HCOOCH}_3$  (A and E) lines (emission) and CN lines (absorption). Right to left are CN  $2_{3/2, 5/2} - 1_{1/2, 3/2}$ ,  $2_{3/2, 1/2} - 1_{1/2, 1/2}$ ,  $2_{3/2, 3/2} - 1_{1/2, 1/2}$ ,  $\text{HCOOCH}_3\text{-E}$  and  $\text{-A } 20_{2,19} - 19_{2,18}$ ,  $\text{HCOOCH}_3\text{-E}$  and  $\text{-A } 20_{1,19} - 19_{1,18}$ .

peak could indeed be part of the line itself, which would be strongly self-absorbed at  $V_{\text{LSR}}=3.9 \text{ km s}^{-1}$ . If this is the case, the linewidths of source B would be  $\sim 4\text{-}6 \text{ km s}^{-1}$  (Fig. 2), similar to the linewidths measured towards source A. Note that the blue peak is expected to be brighter than the red peak in the case of optically thick lines from infalling gas (Leung & Brown 1977; Zhou 1992, 1995; Choi et al. 1995), so it would be consistent with the  $\sim 1 M_{\odot}$  hot corino hypothesis of source B too. This alternative explanation, optically thick lines in source B, is therefore very appealing and worth exploring in some detail. Using the LTE approximation, the required column densities for the  $\text{CH}_3\text{CN}$  and  $\text{HCOOCH}_3$  lines to be optically thick are  $N \sim 10^{16} \text{ cm}^{-2}$  and  $N \sim 10^{17} \text{ cm}^{-2}$  respectively. These values are about one order of magnitude larger than the column density derived in B from the emission lines, assuming that the lines are optically thin, LTE populated and that the emission region fills up the Plateau de Bure synthesized beam (see below). Considering that the three adopted assumptions all underestimate the true column density, it is indeed possible, but not firmly established, that the lines in source B are optically thick. Unfortunately, “physical” considerations

do not help either to distinguish between the two possible interpretations, optically thin or thick lines in source B. In the first case (B has  $V_{\text{LSR}}=2.7 \text{ km s}^{-1}$  and FWHM  $\sim 2 \text{ km s}^{-1}$ ), source B would be less massive than A and would revolve around it at  $1.2 \text{ km s}^{-1}$  (multiplied by the inclination of the orbit), at a distance of 800 AU, which is fully consistent with  $M_A \sim 1 M_{\odot}$  (unless the orbit is in the sky plane). In the second case (B also has  $V_{\text{LSR}}=3.9 \text{ km s}^{-1}$  and FWHM  $\sim 4\text{-}6 \text{ km s}^{-1}$ ), A and B have comparable masses (similar FWHM), but B is more compact. Future high resolution observations of optically thin lines are hence required to definitely settle the question.

As said, the nature of source B affects the determination of the molecular abundances in this source, and hence, how much the chemical composition of the A and B hot corinos differ. Using the relation between column density and observed continuum flux density, and using a dust opacity  $\kappa_{\nu}$  of  $0.8 \text{ cm}^2 \text{ g}^{-1}$  at 1.3 mm and a dust temperature  $T_d$  of 40 K (e.g. Walker et al. 1986), we derive molecular hydrogen column densities from the 1.3 mm continuum emission equal to  $N(\text{H}_2, \text{A}) = 3.5 \times 10^{24} \text{ cm}^{-2}$  in A and  $N(\text{H}_2, \text{B}) = 1.7 \times 10^{25} \text{ cm}^{-2}$  in B (consistent with the values of Mundy et al. (1992)<sup>10</sup>). Using these values and the  $\text{CH}_3\text{CN}$  total column densities derived from the rotational diagram method ( $N_A = 1.7 \times 10^{15} \text{ cm}^{-2}$  and  $N_B = 3.9 \times 10^{14} \text{ cm}^{-2}$ ), we get  $\text{CH}_3\text{CN}$  abundances of  $4.8 \times 10^{-10}$  and  $2.3 \times 10^{-11}$  for A and B respectively, i.e.  $\text{CH}_3\text{CN}$  is  $\sim 20$  times more abundant in A than in B. A rotational diagram could not be drawn for the  $\text{HCOOCH}_3$  transitions as they have similar upper energy levels, but assuming  $T_{\text{rot}} \sim 60 \text{ K}$  (Cazaux et al. 2003) we get  $\text{HCOOCH}_3$  column densities of  $N_A = 2.6 \times 10^{16} \text{ cm}^{-2}$  and  $N_B = 8.4 \times 10^{15} \text{ cm}^{-2}$ , i.e.  $\text{HCOOCH}_3$  abundances of  $7.5 \times 10^{-9}$  and  $4.9 \times 10^{-10}$  for A and B respectively, a factor 15 difference<sup>11</sup>. Note, however, that since B is unresolved in the line emission, and the lines could be optically thick (see above discussion), the molecular abundances quoted for B may be underestimated by about an order of magnitude (note also that the region of molecular emission could be more compact than the continuum emission region). Therefore, resolving the problem of the nature of the observed line emission in source B is crucial, not only to determine the dynamical state of this source, but also to correctly assess the difference in the chemical composition of sources A and B.

In summary, these interferometric observations with the Plateau de Bure show unambiguously that the observed complex organic molecules are emitted from two compact ( $\leq 1.5''$ ) regions, which is consistent with grain mantle evaporation. No indication was found in support of other formation mechanisms for these molecules. Two scenarios have been proposed to explain the observed differences in sources A and B. However, the available data are insufficient to fully understand how and why the two components differ in their dynamical and chemical state, and more interferometric observations (e.g. of optically thin lines) are needed in order to solve the issues raised in this Letter.

<sup>10</sup> We postpone the detailed analysis of the continuum emission to a forthcoming paper.

<sup>11</sup> Note that the abundances quoted in Cazaux et al. differ from those derived here because of the different estimate of the  $\text{H}_2$  column density.

## REFERENCES

- Arce, H. G. & Sargent, A. I. 2004, *ApJ*, 612, 342
- Bottinelli, S., Ceccarelli, C., Lefloch, B., Williams, J. P., Castets, A., Caux, E., Cazaux, S., Maret, S., Parise, B. & Tielens, A. G. M. 2004, *ApJ*, v.612 in press
- Cazaux, S., Tielens, A. G. G. M., Ceccarelli, C., Castets, C. Wakelam, V., Caux, E., Parise, B., & Teyssier, D. 2003, *ApJ*, 593, L51
- Ceccarelli, C. 2004, in *Star Formation in the Interstellar Medium*, eds. D. Johnstone & D. Lin (ASP Conference Series)
- Ceccarelli, C., Castets, A., Caux, E., Hollenbach, D., Loinard, L., Molinari, S., & Tielens, A. G. G. M. 2000a, *A&A*, 355, 1129
- Ceccarelli, C., Loinard, L., Castets, A., Tielens, A. G. G. M., & Caux, E. 2000b, *A&A*, 357, L9
- Choi, M., Evans, N. J. II, Gregersen, E. M., & Wang, Y. 1995, *ApJ*, 448, 742
- Doty, S. D., Schöier, F. L., & van Dishoeck, E. F. 2004, *A&A*, 418, 1021
- Kurtz, S., Cesaroni, R., Churchwell, E., Hofner, P., & Walmsley, C. M. 2000, in *Protostars and Planets IV*, eds V. Mannings, A. P. Boss, S. S. Russell, (Tucson: University of Arizona Press), 299
- Leung, C. M. & Brown, R. L. 1977, *ApJ*, 214, L73
- Looney, L. W., Mundy, L. G., & Welch, W. J. 2000, *ApJ*, 529, 477
- Maret, S., Ceccarelli, C., Caux, E., Tielens, A. G. G. M., Jørgensen, J. K., van Dishoeck, E., Bacmann, A., Castets, A., Lefloch, B., Loinard, L., Parise, B., & Schöier, F. L. 2004, *A&A* 416, 577
- Maret, S., Ceccarelli, C., Caux, E., Tielens, A. G. G. M. & Castets, A. 2002, *A&A*, 395, 573
- Mezger, P. G., Wink, J. E., & Zylka, R. 1990, *A&A*, 228, 95
- Mundy, L. G., Wootten, A., Wilking, B. A., Blake, G. A., & Sargent, A. I. 1992, *ApJ*, 385, 306
- Mundy, L. G., Wootten, H. A., & Wilking, B. A. 1990, *ApJ*, 352, 159
- Schöier, F. L., Jørgensen, J. K., van Dishoeck, E. F., & Blake, G. A. 2004, *A&A*, 418, 185
- Schöier, F. L., Jørgensen, J. K., van Dishoeck, E. F., & Blake, G. A. 2002, *A&A*, 390, 1001
- van Dishoeck, E. F. & Blake, G. A. 1998, *ARAAS*, 36, 317
- Wooten, H. A. 1989, *ApJ*, 337, 858
- Zhou, S. 1995, *ApJ*, 442, 685
- Zhou, S. 1992, *ApJ*, 394, 204